Analysis of Transient Electromagnetic Scattering from Closed Surfaces Using a Combined Field Integral Equation

Balasubramaniam Shanker, *Member, IEEE*, A. Arif Ergin, *Student Member, IEEE*, Kemal Aygün, *Student Member, IEEE*, and Eric Michielssen, *Senior Member, IEEE*

***Abstract*—In the past, both the time-domain electric and magnetic field integral equations have been applied to the analysis of transient scattering from closed structures. Unfortunately, the solutions to both these equations are often corrupted by the presence of spurious interior cavity modes. In this article, a time-domain combined field integral equation is derived and shown to offer solutions devoid of any resonant components. It is anticipated that stable marching-on-in-time schemes for solving this combined field integral equation supplemented by fast transient evaluation schemes such as the plane wave time-domain algorithm will enable the analysis of scattering from electrically large closed bodies capable of supporting resonant modes.**

***Index Terms*—Integral equations, transient electromagnetic scattering.**

I. Introduction

In recent years, the electromagnetics community has pursued with renewed vigor the development of efficient transient simulators. These simulators rely on either differential or integral equation formulations and aim to accurately and efficiently characterize broad-band and nonlinear systems. Historically, differential-equation methods for analyzing electromagnetic transients have been favored over their integral equation counterparts [1]. When applied to the analysis of volume scattering problems, differential-equation-based methods offer unquestionable advantages over integral equation techniques. However, when analyzing surface scattering phenomena, the advantages of differential equation approaches over integral equation techniques fade. Indeed, integral equation methods only require a discretization of the scatterer surface as opposed to a volume surrounding the scatterer and do not call for absorbing boundary conditions, but automatically impose the radiation condition.

Their intrinsic qualities notwithstanding, time-domain integral-equation (TDIE) methods have not enjoyed widespread application, even in the study of surface scattering phenomena. Two principal hurdles have impeded their general acceptance. First, historically, many marching-on-in-time (MOT) methods for solving TDIEs have been shown prone to late-time instabilities. While it has been known for several years that these instabilities can be partially remedied through spatial and temporal filtering [2]–[5], it was not until recently that Bluck and Walker demonstrated that judiciously constructed MOT schemes relying on accurate spatial integration rules and implicit time-stepping schemes are for all practical purposes stable [6], [7]. While [6] and [7] arrive at this conclusion for MOT schemes designed to solve magnetic field integral equations (MFIEs), it has been reported that MOT schemes for solving electric field integral equations (EFIEs) can likewise be "stabilized," albeit with a little more difficulty [8]–[11]. Second, the cost associated with the application of traditional MOT schemes scales unfavorably with problem size. Indeed, the computational complexity of classical MOT schemes scales as $O(N_t N_s^2)$, where N_s is the number of surface unknowns and N_t is the number of time steps (for a surface scatterer N_t typically scales as $\sqrt{N_s}$). This scaling law renders the analysis of electrically large structures using a classical MOT algorithm practically impossible with current computational resources. However, recently, an algorithm that considerably reduces the computational complexity of conventional MOT schemes was proposed. Specifically, it was shown that the computational cost of an MOT analysis is reduced from $O(N_t N_s^2)$ to $O(N_t N_s^{1.5} \log N_s)$ and $O(N_t N_s \log^2 N_s)$ when the MOT scheme is supplemented by two-level [12]–[14] and multilevel plane wave time-domain (PWTD) algorithms [15], [16], respectively. It is anticipated that these two developments, viz., the construction of implicit MOT schemes and PWTD accelerators will result in a more widespread acceptance of TDIE techniques as viable alternatives to differential equation methods for analyzing transient surface scattering phenomena.

In the past, both the time-domain MFIE and EFIE have been extensively used to analyze transient scattering from closed surfaces. As was pointed out before, most MOT schemes for solving these equations were found to be unstable. Ever since the insightful studies of Rynne and Smith [3] and Smith [17], cavity resonances have been suspected of contributing to these instabilities. These authors definitively conclude that MOT instabilities arise when the singularity expansion method poles that characterize the resolvent of the integral equation being solved drift into the right half-plane due to the approximations introduced by the numerical scheme. Needless to say, poles describing interior resonances permitted by the

Manuscript received October 14, 1998; revised February 8, 2000. This work was supported in part by an AFOSR Grant via the MURI Program under Contract F49620-96-1-0025, NSF Grant ECS 95-02138, and the Gebze Institute of Technology, Turkey.

The authors are with the Center for Computational Electromagnetics, Department of Electrical and Computer Engineering, University of Illinois at Urbana–Champaign, Urbana, IL 61801 USA (e-mail: shanker@socrates.ece.uiuc.edu).

Publisher Item Identifier S 0018-926X(00)06937-4.

time domain MFIE and EFIE are prime candidates for such undesirable shifts as they reside on the imaginary axis. It is now known that carefully constructed implicit methods for solving the time-domain MFIE are virtually always stable (and, therefore, appear to largely avoid such undesirable pole displacements; unfortunately, a similar statement cannot be made about EFIEs). While this progress is exciting, it does not mean that MOT-based schemes for solving these integral equations always yield accurate results. Indeed, while in theory the cavity poles of a closed body are never excited upon external illumination [18], practical numerical schemes will develop solutions that contain components corresponding to these (slightly perturbed) resonances [3]. The excitation of the modes described by these poles does not necessarily lead to instabilities, but does result in inaccurate solutions.

This article presents a study on a resonance suppressing scheme for TDIE solutions. The issue has gained new relevance with the availability of implicit and fast TDIE techniques capable of analyzing scattering from large-scale objects that possibly support resonances. In tackling this problem, we build on the vast body of research on this topic in frequency-domain analysis. It is well known that the solutions to both the frequency-domain EFIE and MFIE can be corrupted when the frequency of the incident field approaches that of one of the scatterer's resonant modes. It is also known that this interior resonance problem can be remedied using a variety of approaches. Chief among those and perhaps most widely accepted is the use of a frequency-domain combined field integral equation (CFIE) [19], [20].

In this paper, a time-domain CFIE for analyzing scattering from three-dimensional perfect electrically conducting (PEC) closed surfaces is presented. It is argued that the proposed CFIE eliminates the interior cavity modes that possibly corrupt the solutions to the EFIE and MFIE. Indeed, it is experimentally verified that the solutions to both the time domain EFIE and MFIE are prone to inaccuracies resulting from interior resonances as practical MOT schemes for solving these equations develop nonphysical resonant currents. Finally, it is experimentally demonstrated that implicit MOT schemes relying on accurate temporal and spatial integration rules for solving the proposed CFIE remove all nonphysical resonant components from the solution and, hence, constitute a stable and viable approach for analyzing transient scattering from electrically large objects.

This paper is organized as follows. In Section II various time-domain integral equations (including the proposed CFIE) are presented and their properties discussed. An MOT scheme for solving the CFIE is also outlined. Section III provides a plethora of numerical results that demonstrate the efficacy of the proposed method in eliminating nonphysical currents corresponding to resonant modes that plague time-domain EFIE- and MFIE-based approaches. Finally, Section IV presents our conclusions.

II. Formulation

In this section, a time-domain CFIE for analyzing scattering from closed structures is introduced. An MOT-based scheme for solving this equation is also outlined.

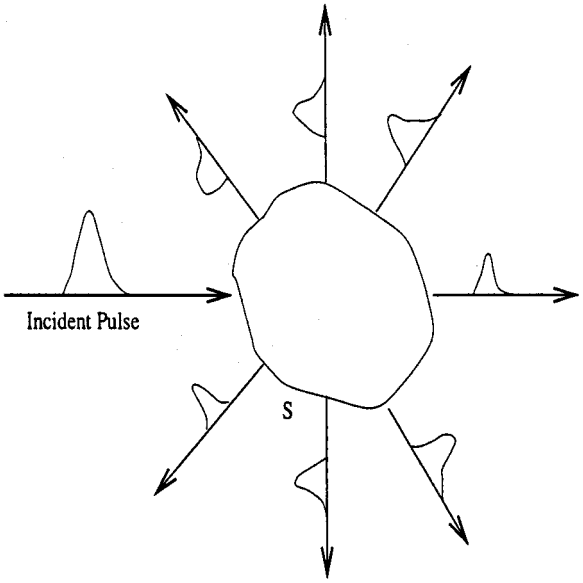

Fig. 1. Description of the problem.

A. Time-Domain Integral Equations

Let S denote the surface of a closed perfectly conducting body that resides in free-space and that is excited by a transient electromagnetic field $\{\boldsymbol{E}^i(\boldsymbol{r}, t), \boldsymbol{H}^i(\boldsymbol{r}, t)\}$ (Fig. 1). The interaction of the incident field with S results in a surface current $\boldsymbol{J}(\boldsymbol{r}, t)$, which in turn generates a scattered electromagnetic field $\{\boldsymbol{E}^s(\boldsymbol{r}, t), \boldsymbol{H}^s(\boldsymbol{r}, t)\}$. These fields are fully characterized by the vector and scalar potentials defined as

$$\boldsymbol{A}(\boldsymbol{r}, t) = \frac{\mu_0}{4\pi} \int_S dS' \frac{\boldsymbol{J}(\boldsymbol{r}', \tau)}{R} \tag{1a}$$

and

$$\Phi(\boldsymbol{r}, t) = \frac{1}{4\pi\epsilon_0} \int_S dS' \frac{\sigma(\boldsymbol{r}', \tau)}{R} \tag{1b}$$

where

$R = \lvert\boldsymbol{R}\rvert\lvert\boldsymbol{r} - \boldsymbol{r}'\rvert$	distance between the source and observation points;
$\tau = t - R/c$	retarded time;
c	speed of light;
ϵ_0 and μ_0	permittivity and permeability of free-space, respectively.

Also, $\sigma(\boldsymbol{r}, t)$ denotes the surface charge density that is related to $\boldsymbol{J}(\boldsymbol{r}, t)$ through the continuity equation

$$\nabla \cdot \boldsymbol{J}(\boldsymbol{r}, t) + \partial_t \sigma(\boldsymbol{r}, t) = 0. \tag{2}$$

In what follows, surfaces conformal to S (but residing just outside and just inside S) are denoted by S_+ and S_-, respectively, and $\hat{\boldsymbol{n}}$ denotes an outward pointing and position-dependent unit normal to S.

To arrive at a time-domain EFIE, note that the scattered electric field $\boldsymbol{E}^s(\boldsymbol{r}, t)$ can be expressed in terms of the above potentials as

$$\boldsymbol{E}^s(\boldsymbol{r}, t) = -\partial_t \boldsymbol{A}(\boldsymbol{r}, t) - \nabla\Phi(\boldsymbol{r}, t). \tag{3}$$

The incident field $\boldsymbol{E}^i(\boldsymbol{r}, t)$ can be related to the scattered field by enforcing the boundary condition that the total electric field $\boldsymbol{E}^t(\boldsymbol{r}, t) = \boldsymbol{E}^i(\boldsymbol{r}, t) + \boldsymbol{E}^s(\boldsymbol{r}, t)$ tangential to S vanishes

$$\hat{\boldsymbol{n}}\times\hat{\boldsymbol{n}}\times\boldsymbol{E}^i(\boldsymbol{r}, t) = -\hat{\boldsymbol{n}}\times\hat{\boldsymbol{n}}\times\boldsymbol{E}^s(\boldsymbol{r}, t) \quad \forall \boldsymbol{r} \in S, S_+, S_-. \tag{4}$$

The same condition holds true on both S_- and S_+. Hence, using (1)–(3) in (4) the following EFIE for $\boldsymbol{J}(\boldsymbol{r}, t)$ is obtained:

$$\left.\begin{aligned} &\hat{\boldsymbol{n}} \times \hat{\boldsymbol{n}} \times \boldsymbol{E}^i(\boldsymbol{r}, t) \\ &= \hat{\boldsymbol{n}} \times \hat{\boldsymbol{n}} \times \left\{ \frac{\mu_0 \partial_t}{4\pi} \int_S dS' \frac{\boldsymbol{J}(\boldsymbol{r}', \tau)}{R} \right. \\ &\qquad - \frac{\nabla}{4\pi\epsilon_0} \int_S dS' \int_{-\infty}^{\tau} \\ &\qquad \left. \cdot\, dt \frac{\nabla' \cdot \boldsymbol{J}(\boldsymbol{r}', t)}{R} \right\} \\ &\doteq \mathcal{L}_e\{\boldsymbol{J}(\boldsymbol{r}', t)\} \end{aligned}\right\} \forall \boldsymbol{r} \in S, S_+, S_-. \tag{5}$$

The $\mathcal{L}_e$ defined in the above equation will henceforth be referred to as the electric field operator.

Likewise, a time-domain MFIE can be derived by expressing the scattered magnetic field as

$$\boldsymbol{H}^s(\boldsymbol{r}, t) = \frac{1}{\mu_0} \nabla \times \boldsymbol{A}(\boldsymbol{r}, t) \tag{6}$$

and by enforcing the condition that the total magnetic field $\boldsymbol{H}^t(\boldsymbol{r}, t) = \boldsymbol{H}^i(\boldsymbol{r}, t) + \boldsymbol{H}^s(\boldsymbol{r}, t)$ tangential to S_- vanishes, i.e.,

$$\hat{\boldsymbol{n}} \times \boldsymbol{H}^i(\boldsymbol{r}, t) = -\hat{\boldsymbol{n}} \times \boldsymbol{H}^s(\boldsymbol{r}, t) \quad \forall \boldsymbol{r} \in S_-. \tag{7}$$

Upon using (1a) together with (6) in (7), the following MFIE for $\boldsymbol{J}(\boldsymbol{r}, t)$ results

$$\left.\begin{aligned} &\hat{\boldsymbol{n}} \times \boldsymbol{H}^i(\boldsymbol{r}, t) \\ &= -\frac{1}{4\pi} \hat{\boldsymbol{n}} \times \int_S dS' \\ &\qquad \cdot \left[\frac{1}{cR} \partial_t \boldsymbol{J}(\boldsymbol{r}', \tau) + \frac{1}{R^2} \boldsymbol{J}(\boldsymbol{r}', \tau) \right] \times \hat{\boldsymbol{R}} \\ &\doteq \mathcal{L}_h\{\boldsymbol{J}(\boldsymbol{r}', t)\} \end{aligned}\right\} \forall \boldsymbol{r} \in S_- \tag{8}$$

where $\hat{\boldsymbol{R}} = \boldsymbol{R}/R$. Henceforth, the $\mathcal{L}_h$ defined in the above equation will be referred to as the magnetic field operator.

The singularity expansion method shows that the solution to the homogeneous time-domain EFIE and MFIE is characterized by the poles of the resolvent of $\mathcal{L}_e$ and $\mathcal{L}_h$ [18], respectively. Of course, some of these poles lie close to the right half-plane and those on the imaginary axis correspond to the frequencies of the interior cavity modes that the EFIE and MFIE support. It has been established that in theory the incident field does not couple to the interior modes [18]. Unfortunately, because of two important effects, the situation changes drastically when (5) and (8) are solved numerically. First, inaccuracies inherent to a numerical scheme will result in shifting of the system poles, some of which may end up in the right half-plane, which is problematic because this leads to instabilities. It has been argued that as the inaccuracies are more substantial at higher frequencies, the movement of the poles associated with these frequencies will be larger [3], [17]. Explicit MOT schemes lead to larger pole displacement which renders these techniques virtually always unstable. In contrast, Bluck and Walker [6] experimentally demonstrate that implicit schemes are for all practical purposes stable, which implies that these schemes avoid pole displacement into the right half-plane. Second, in a numerical framework, the incident field does couple to the perturbed interior modes that are supported by the EFIE and MFIE. While this does not necessarily lead to unstable behavior when implicit methods are used, it does follow that the solution can be corrupted by the presence of perturbed cavity modes. The actual level of excitation of these modes depends heavily on the details of the implementation. Bluck and Walker [6] report schemes that appear rather insensitive though not totally immune to the excitation of these resonance. In contrast, as will be demonstrated in Section III (numerical results), our flat-panel triangular-patch implicit MOT implementation does pick up resonances, albeit often in only minute quantities. However, we conjecture that any EFIE/MFIE implementation will pick up these modes provided that the incident pulse contains sufficient energy in the frequency band near these resonances.

To combat this resonance problem, a time-domain CFIE is constructed in analogy to its frequency-domain counterpart by combining the EFIE and MFIE as

$$-\beta/\eta_0 \hat{\boldsymbol{n}} \times \hat{\boldsymbol{n}} \times \boldsymbol{E}^t(\boldsymbol{r}, t) + \hat{\boldsymbol{n}} \times \boldsymbol{H}^t(\boldsymbol{r}, t) = 0 \quad \forall \boldsymbol{r} \in S_- \tag{9}$$

where $\eta_0 = \sqrt{\mu_0/\epsilon_0}$ is the intrinsic impedance of the free-space, introduced in (9) for scaling purposes and β is a (real) constant that is greater than zero. In terms of incident and scattered fields, the above equation can be stated as

$$\left.\begin{aligned} &-\beta/\eta_0 \hat{\boldsymbol{n}} \times \hat{\boldsymbol{n}} \times \boldsymbol{E}^i(\boldsymbol{r}, t) + \hat{\boldsymbol{n}} \times \boldsymbol{H}^i(\boldsymbol{r}, t) \\ &= -\beta/\eta_0 \mathcal{L}_e\{\boldsymbol{J}(\boldsymbol{r}', t)\} + \mathcal{L}_h\{\boldsymbol{J}(\boldsymbol{r}', t)\} \\ &\doteq \mathcal{L}_c\{\boldsymbol{J}(\boldsymbol{r}', t)\} \end{aligned}\right\} \forall \boldsymbol{r} \in S_-. \tag{10}$$

The combined field operator $\mathcal{L}_c\{\boldsymbol{J}(\boldsymbol{r}, t)\}$ is a linear combination of the electric and magnetic field operators $\mathcal{L}_e\{\boldsymbol{J}(\boldsymbol{r}, t)\}$ and $\mathcal{L}_h\{\boldsymbol{J}(\boldsymbol{r}, t)\}$.

As pointed out before, when numerically solving (5) and (8), poles corresponding to the resonance frequencies of the cavity formed by S can be excited. On the other hand, our numerical results indicate that, for all structures tested the solution to the CFIE is free of cavity modes. As with the frequency domain CFIE [18] $\beta > 0$ resulted in a resonant free solution.

An earlier investigation into the use of the CFIE was presented by Vechinski and Rao in [21]. There, the authors used

$$\begin{aligned} &-\beta/\eta_0 \hat{\boldsymbol{n}} \times \hat{\boldsymbol{n}} \times \partial_t \boldsymbol{E}^i(\boldsymbol{r}, t) + \hat{\boldsymbol{n}} \times \partial_t \boldsymbol{H}^i(\boldsymbol{r}, t) \\ &\quad = \partial_t \mathcal{L}_c\{\boldsymbol{J}(\boldsymbol{r}', t)\} \quad \forall \boldsymbol{r} \in S_- \end{aligned} \tag{11}$$

for the analysis of two-dimensional (2-D) scattering instead of (10). The purpose of the analysis presented in [21] was to determine whether the late-time instabilities commonly encountered in MOT schemes that rely on explicit time stepping can be overcome by using a combined field formulation. In this regard, no benefit from using a CFIE was observed. This can again be explained using the arguments put forth by Rynne and Smith [3]. A CFIE formulation only eliminates the poles that

lie on the imaginary axis corresponding to the interior cavity modes and does not affect the location of the poles describing the exterior problem. As the MOT scheme prescribed in [21] relies on an explicit time-marching scheme, it is conjectured that the poles of the resolvent of $\partial_t \mathcal{L}_c$ that lie close to the imaginary axis easily shift into the right half-plane, thereby generating instabilities. As a result, little benefit is observed from using a resonance suppressing integral equation method. Finally, experiments indicate that our implicit time stepping scheme for solving (10) (see Section II-B) yields a more accurate solution than that of (11), based upon otherwise very similar implementation choices; it is for this reason that in this work (10) was selected over (11).

B. MOT Algorithm

Equation (10) can be solved numerically by adopting a discrete representation for the current $\boldsymbol{J}(\boldsymbol{r}, t)$ and by discretizing the CFIE accordingly. Following standard practice, the scatterer is modeled by flat triangular facets and the current $\boldsymbol{J}(\boldsymbol{r}, t)$ is represented using spatial and temporal basis functions $\boldsymbol{j}_n(\boldsymbol{r})$ for $n = 1, \cdots, N_s$ and $T_j(t)$ for $j = 0, \cdots, N_t$ such that

$$\boldsymbol{J}(\boldsymbol{r}, t) = \sum_{j=0}^{N_t} \sum_{n=1}^{N_s} I_{n,j} \boldsymbol{j}_n(\boldsymbol{r}) T_j(t) \tag{12}$$

where $I_{n,j}$ is the weight associated with the space–time basis function $\boldsymbol{j}_n(\boldsymbol{r})T_j(t)$. In our implementation, the $\boldsymbol{j}_n(\boldsymbol{r})$ are chosen to be the Rao–Wilton–Glisson (RWG) basis functions, which have been used extensively in the integral-equation-based analysis of both time-harmonic and transient scattering phenomena [22], [23]. The temporal bases $T_j(t) = T(t - j\,\Delta t)$ are assumed to be triangular functions [23]. In other words, $T(t) = 1$ for $t = 0$ linearly interpolates to zero for $t = \pm\Delta_t$ (Δ_t denotes the time-step size) and is zero outside the interval $(-\Delta_t, \Delta_t)$. It is possible to choose higher order spatial and temporal interpolation functions to improve the accuracy and stability of the MOT scheme [6], [8]. By expanding the current density as in (12) and by applying a spatial Galerkin testing procedure at $t = t_j = j\,\Delta_t$, the following matrix equation is obtained:

$$\mathcal{Z}_0 \mathcal{I}_j = \mathcal{F}_j^{inc} - \sum_{l=1}^{j} \mathcal{Z}_l \mathcal{I}_{j-l} \tag{13a}$$

where the entries of the vectors $\mathcal{I}_j$, $\mathcal{F}_j^{inc}$ and the matrices $\mathcal{Z}_l$ are given by

$$\mathcal{I}_{j,m} = I_{m,j} \tag{13b}$$

$$\begin{aligned} \mathcal{F}_{j,m}^{inc} = &-\beta/\eta_0 \langle \boldsymbol{j}_m(\boldsymbol{r}), \hat{\boldsymbol{n}} \times \hat{\boldsymbol{n}} \times \boldsymbol{E}^i(\boldsymbol{r}, t_j) \rangle \\ &+ \langle \boldsymbol{j}_m(\boldsymbol{r}), \hat{\boldsymbol{n}} \times \boldsymbol{H}^i(\boldsymbol{r}, t_j) \rangle \end{aligned} \tag{13c}$$

$$\begin{aligned} \mathcal{Z}_{l,mn} = &-\beta/\eta_0 \langle \boldsymbol{j}_m(\boldsymbol{r}), \mathcal{L}_e\{\boldsymbol{j}_n(\boldsymbol{r}) T_{j-l}(t))\}\rangle|_{t=t_j} \\ &+ \langle \boldsymbol{j}_m(\boldsymbol{r}), \mathcal{L}_h\{\boldsymbol{j}_n(\boldsymbol{r}) T_{j-l}(t))\}\rangle|_{t=t_j}. \end{aligned} \tag{13d}$$

In the above equations, $\langle \phi(\boldsymbol{r}), \xi(\boldsymbol{r}) \rangle = \int_{S^-} dS \phi(\boldsymbol{r}) \cdot \xi(\boldsymbol{r})$ denotes the standard inner product. Equation (13a) is the basis for the classical MOT scheme. Assuming that the currents up to the $(j-1)$th time step are known, this equation permits the computation of the currents associated with the jth time step. Hence, the currents at all time points of interest can be computed recursively.

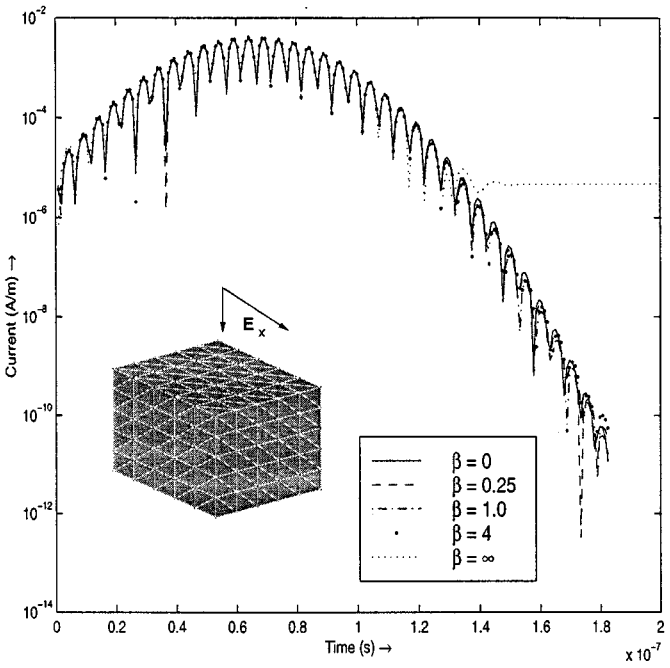

Fig. 2. Comparison of the currents observed on a cube as a function of time. The currents are computed using the time-domain CFIE code for $\beta = 0$ (MFIE), 0.25, 1.0, 4.0, and ∞ (EFIE).

In our practical implementation of this scheme the inner product that appear in (13a), (13c) and (d) are evaluated using seven-point Gaussian quadrature [24]. This leads to an implicit scheme even for very small time-step sizes, however, in all our calculations we use $\Delta_t = 1/(10 f_{\max})$. This choice of time-step size results in $\mathcal{Z}_0$ being a highly sparse matrix; for very regular structures the number of entries in each row is approximately $\mathcal{O}(1)$. Equation (13a) is then solved using a nonstationary iterative solver such as the transpose-free quasi minimal residual (TFQMR) method [25].

It has been observed that the MOT scheme for solving the MFIE is easier to stabilize than that for the EFIE. The studies of Manara *et al.* [8] and Rao and Sarkar [10] notwithstanding, we have found that implicit schemes and accurate integration rules do not guarantee stability when the spectrum of the incident pulse contains the resonance frequencies of the scatterer. To combat this EFIE instability, averaging as suggested by Rynne and Smith [3] is used, though it should be stressed, only for the EFIE. On the other hand, MOT schemes for solving the CFIE and MFIE have been found to be always stable as long as implicit time-stepping methods and accurate integration rules are used.

III. Numerical Results

The objective of this section is to demonstrate that the above proposed time-domain CFIE yields solutions uncorrupted by the presence of cavity modes even when the spectrum of the incident pulse includes one or more of the scatterer's resonance frequencies. As a first step toward validating our codes, the current

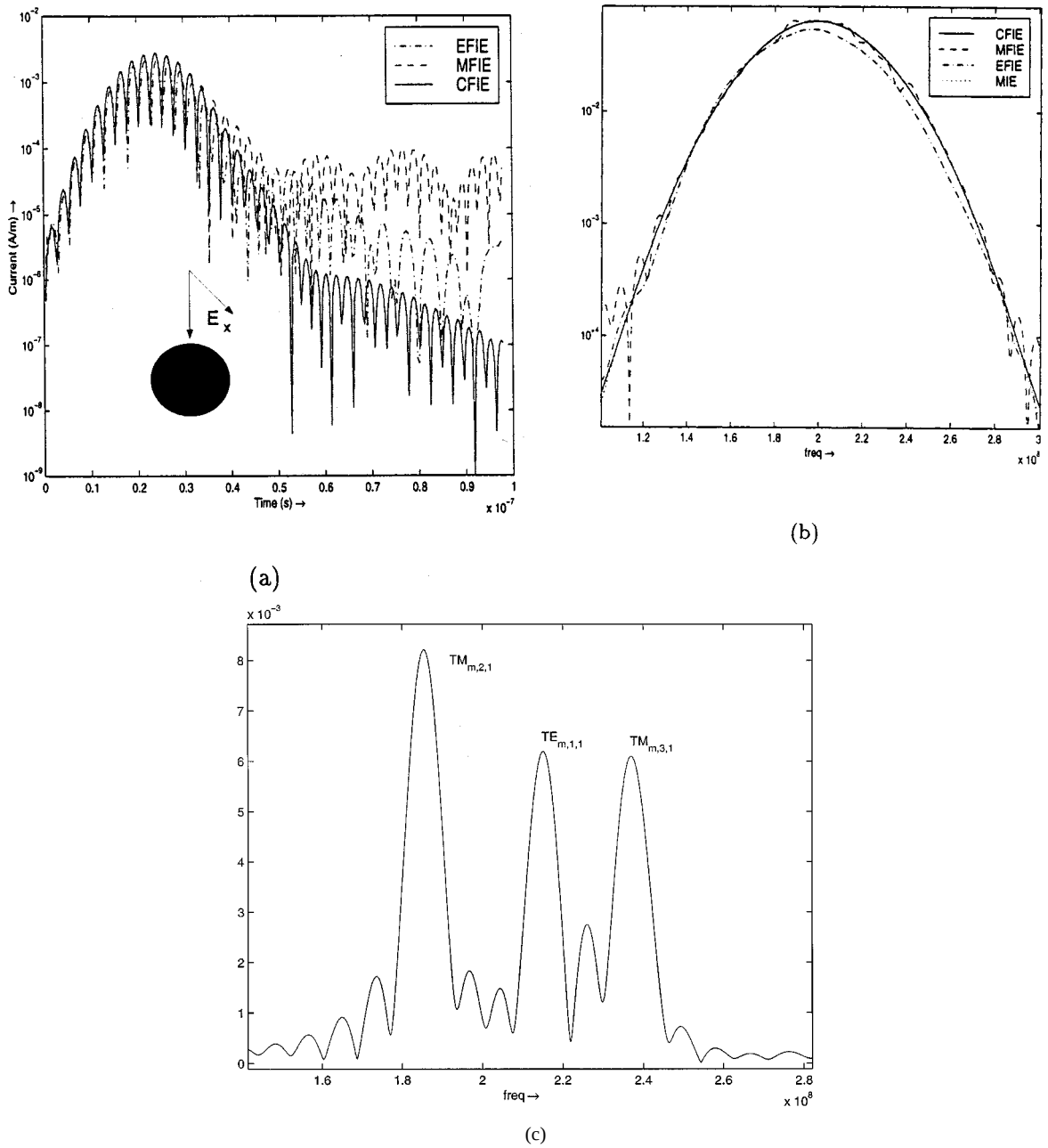

Fig. 3. (a) Comparison of the current observed at a point on a sphere computed using MFIE, EFIE and CFIE ($\beta = 0.2$). (b) Comparison of the absolute value of the Fourier transform of these currents. (c) The absolute value of the Fourier transform of the difference between the currents computed using the time-domain CFIE and MFIE.

on an electrically small structure obtained using the CFIE code will be compared against those obtained using codes based upon the EFIE and MFIE presented in (5) and (8), respectively. In this experiment, it will be ensured that no resonant modes are excited by virtue of the choice of dimensions of the scatterer with respect to the wavelength at the highest frequency present in the incident pulse (delineated by the notion of bandwidth to be introduced shortly). Next, the currents on and the far-field signatures of electrically large structures will be computed using the time-domain CFIE code. The far-field signatures will then be Fourier transformed into the frequency domain and the object's radar cross section (RCS) will be extracted at several frequencies. These results will then be compared against the RCS computed using FISC (fast Illinois solver code), a frequency domain fast multipole-based CFIE code that has been extensively validated [26]. To give a more quantitative feel to figures containing these comparisons, root mean square (rms) deviations of results obtained using time-domain codes from those obtained using FISC (or analytical results where available) over a range of angles are given to demonstrate the relative errors of the three approaches. The incident pulse used in all the examples that follow is a modulated Gaussian given by

$$\boldsymbol{E}^i(\boldsymbol{r}, t) = \hat{\boldsymbol{p}} \cos(2\pi f_0 \tau) \exp\left[-\frac{(\tau - t_p)^2}{2\sigma^2}\right] \qquad (14)$$

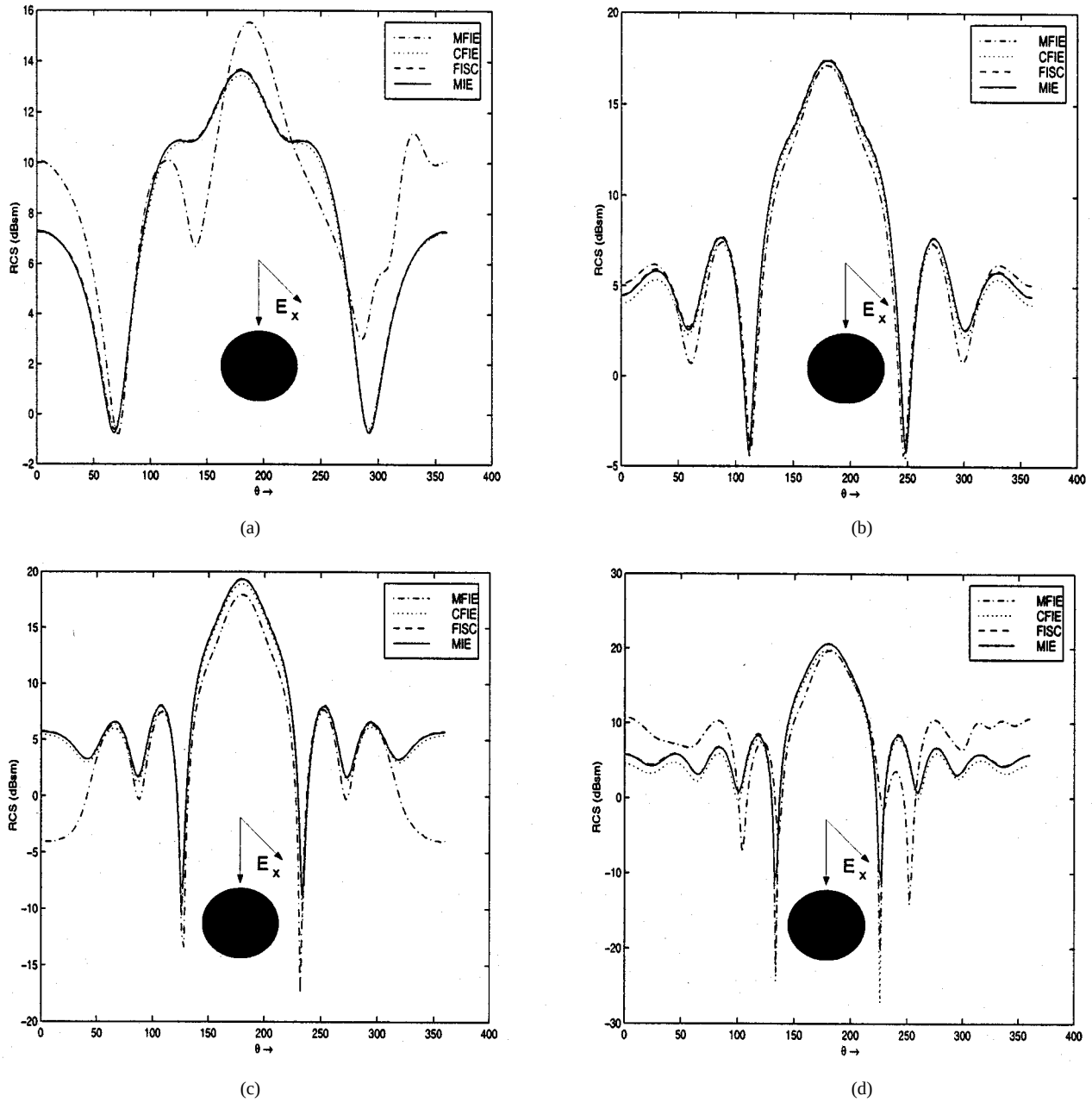

Fig. 4. The radar scattering cross section of a sphere in the x–z plane extracted from the time-domain CFIE and MFIE is compared to that obtained from FISC for four different frequencies. The incident wave propagates along $\hat{\boldsymbol{k}} = -\hat{z}$ and is $\hat{\boldsymbol{p}} = \hat{\boldsymbol{x}}$ polarized. (a) 120 MHz. (b) 190 MHz. (c) 240 MHz. (d) 280 MHz.

where f_0 is the center frequency, $\tau = t - \boldsymbol{r} \cdot \hat{\boldsymbol{k}}/c$, $\hat{\boldsymbol{k}}$ denotes the direction of travel of the incident wave, and $\hat{\boldsymbol{p}}$ its polarization, $\sigma = 6/(2\pi f_{bw})$, $t_p = 3.5\sigma$, and f_{bw} will be further referred to as the bandwidth of the signal. It is to be noted that the power in the incident pulse is down by 160 dB at $f = f_0 + f_{bw}$ relative to that at f_0. Also, it is well known the operational count of the classical MOT solver scales as $\mathcal{O}(N_t N_s^2)$ where N_t is the duration of the analysis and N_s is the number of spatial samples that the surface is discretized into. The results presented herein were obtained using a DecPC whose peak performance is rated at 500 Mflops and the maximum runtime was about an hour.

To validate the time-domain CFIE against the time-domain MFIE and EFIE, consider a cube of dimensions 1 m $\times$ 1 m $\times$ 1 m shown in the inset in Fig. 2. A modulated Gaussian plane wave with $f_0 = 100$ MHz and $f_{bw} = 40$ MHz, traveling along $\hat{\boldsymbol{k}} = -\hat{\boldsymbol{z}}$ with $\hat{\boldsymbol{p}} = \hat{\boldsymbol{x}}$ is incident on the cube. The cube is discretized into 450 spatial unknowns. It is ensured that $f = f_0 + f_{bw}$ is less than 150 MHz, which is the frequency of the first resonant mode of the cube. In Fig. 2, the magnitude of the current at a point on the cube's upper surface computed using $\beta = 0.0$ (MFIE), 0.25, 1.0, 4.0, ∞ (EFIE), is plotted against time. It is seen that the temporal signatures of the current computed using all values of β agree well with each other. However, unlike the currents computed using the CFIE and MFIE, whose magnitude keeps decreasing with time, those obtained using the EFIE stabilize at a value three orders of magnitude below the peak. This behavior of the EFIE has also been observed by other researchers [5].

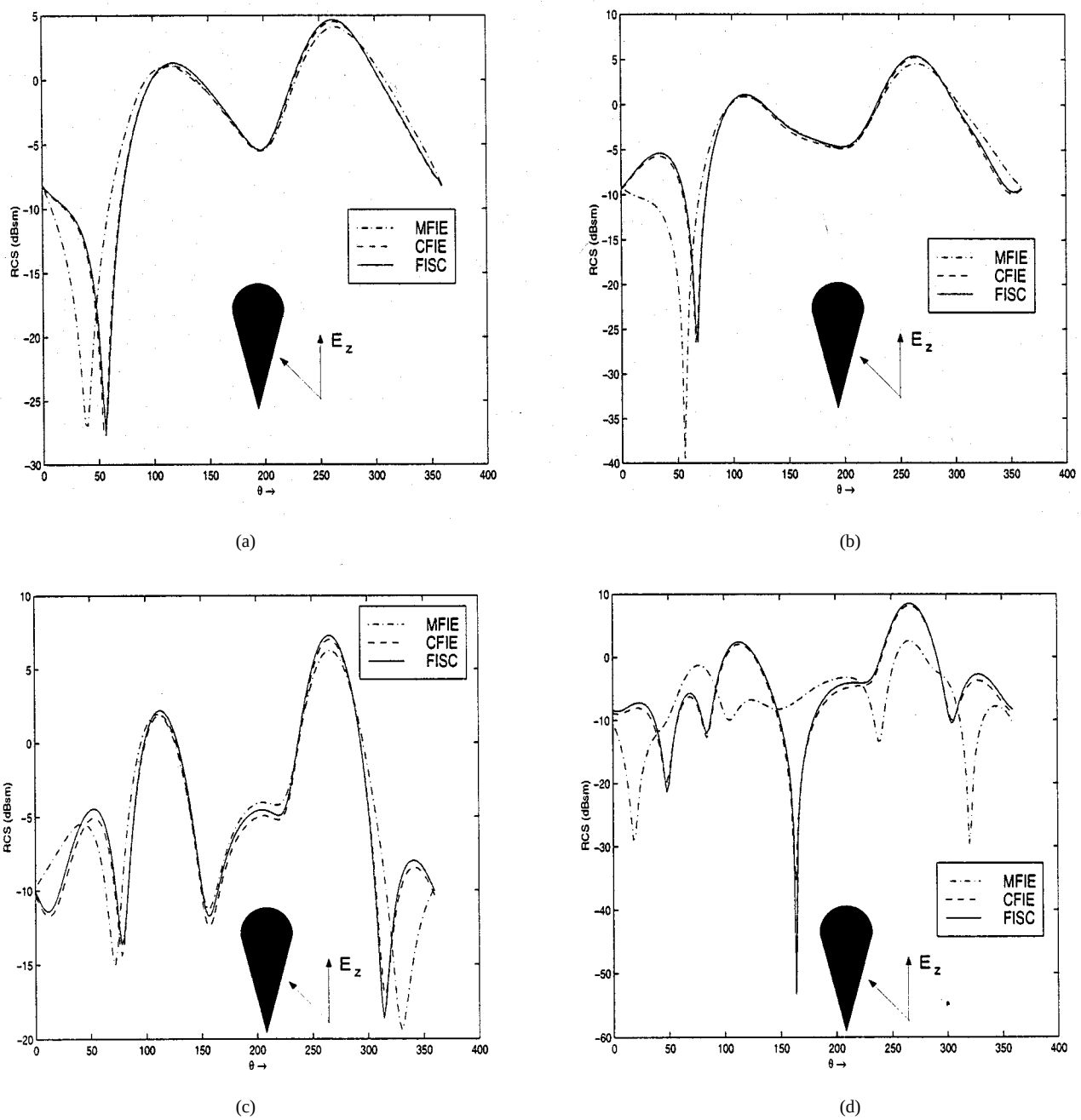

Fig. 5. The radar scattering cross section of a cone sphere in the z–x plane, extracted from the time-domain CFIE and MFIE is compared to that obtained from FISC for a set of frequencies. The incident wave is $\hat{\boldsymbol{p}} = \hat{z}$ polarized and is traveling in the $\hat{\boldsymbol{k}} = -\hat{\boldsymbol{x}}$ direction. (a) 260 MHz. (b) 300 MHz. (c) 400 MHz. (d) 500 MHz.

Having ascertained that the numerical implementation of the time-domain CFIE does yield a solution that coincides with that of the MFIE and the EFIE when no resonant modes are excited, we next examine the CFIE's performance when the spectrum of the incident pulse encompasses the body's resonance frequencies. To this end, consider a sphere of radius 1 m that is discretized using 2793 spatial unknowns, illuminated by a $\hat{\boldsymbol{p}} = \hat{\boldsymbol{x}}$ polarized modulated Gaussian pulse with $\hat{\boldsymbol{k}} = -\hat{\boldsymbol{z}}$. The pulse has a bandwidth of $f_{bw} = 150$ MHz, and a center frequency of $f_0 = 200$ MHz. The above choice of center frequency and bandwidth is such that the $\mathrm{TM}_{m,2,1}$ (184 MHz), $\mathrm{TE}_{m,1,1}$ (214 MHz) and $\mathrm{TM}_{m,3,1}$ (237 MHz) modes are excited. While the sphere theoretically also resonates at $f = 131, 275, 289, 292, 333, 340$ MHz, etc., these modes are barely excited as the power in the incident pulse at these frequencies is down by at least 30 dB from its peak at f_0. The magnitudes of the current at a point on the sphere with $\{\theta = 65°, \phi = 72°\}$ obtained using the EFIE, MFIE, and CFIE ($\beta = 0.25$) codes are compared in Fig. 3(a). It is apparent that the solution to the MFIE exhibits a characteristic ringing, whereas that of the CFIE dies down. As mentioned earlier, since the spectrum of the incident pulse contains resonance frequencies characteristic of the body, it was necessary to use four-point temporal averaging [3] in addition to implicit time

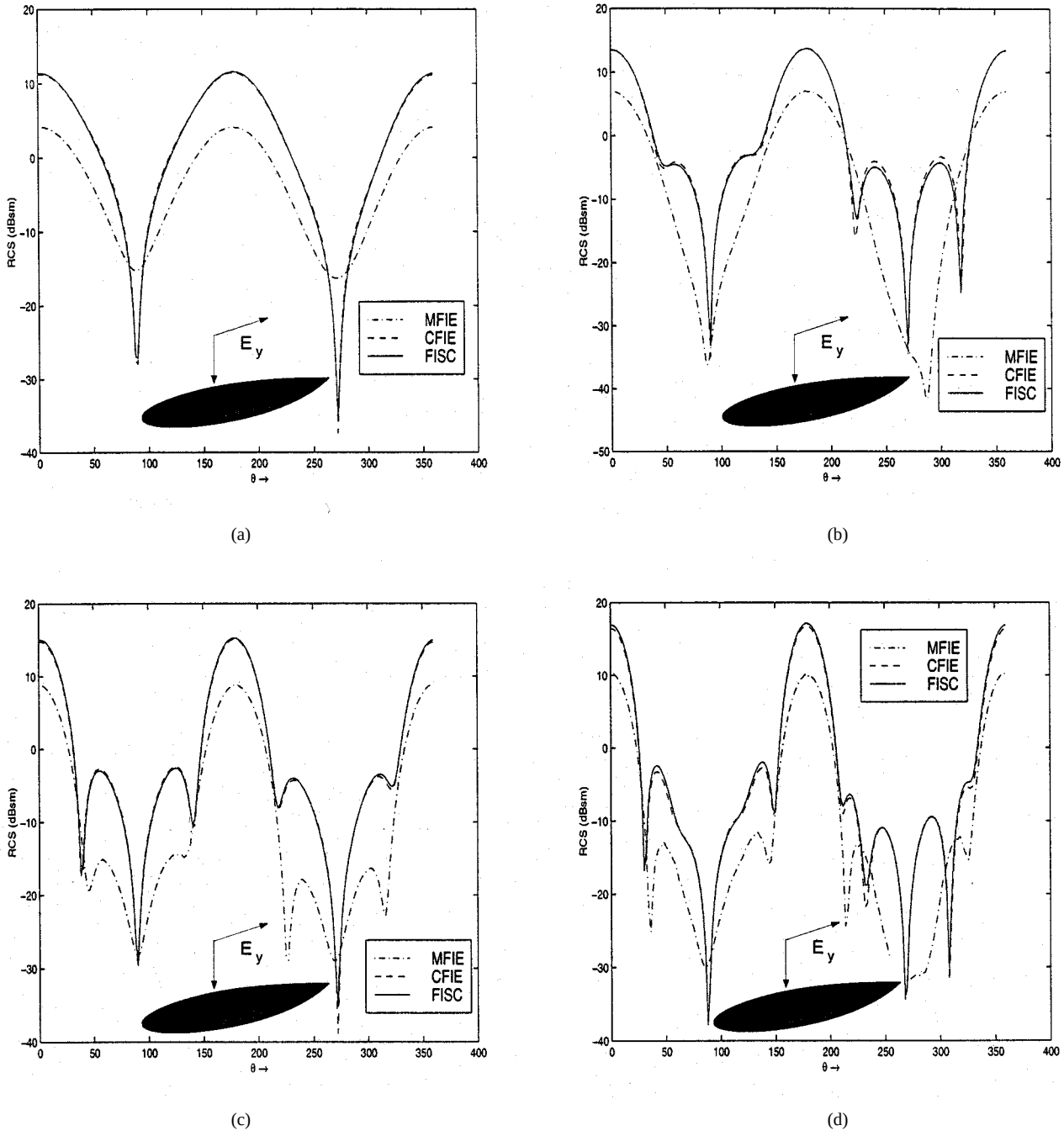

Fig. 6. The radar scattering cross section of an almond in the z–y plane, extracted from the time-domain CFIE and MFIE, is compared to that obtained from FISC for a set of frequencies. The incident wave is $\hat{\boldsymbol{p}} = \hat{\boldsymbol{y}}$ polarized and is traveling in the $\hat{\boldsymbol{k}} = -\hat{z}$ direction. (a) 120 MHz. (b) 150 MHz. (c) 200 MHz. (d) 250 MHz.

stepping to stabilize the solution to the EFIE. As a consequence of using the averaging process, which suppresses resonance effects to some extent, the EFIE solution does not exhibit the same features as that of the MFIE. However, both are still quite different from that obtained using the CFIE. The differences between the currents are further highlighted by examining their Fourier transforms. Fig. 3(b) compares the Fourier transforms of the current obtained using the CFIE, MFIE, and EFIE with those obtained analytically (using Mie series). As is apparent, the CFIE and analytical solutions agree very well with each other, whereas the the others do not; indeed, the variation of the results obtained using the CFIE, MFIE, and the EFIE from the analytical solutions is 0.7%, 7%, and 18%, respectively. The MFIE results are significantly different from the CFIE in the vicinity of the above mentioned resonance frequencies. Also, the Fourier transform of the current obtained using the EFIE is slightly smaller than that obtained using the CFIE and is distorted at the ends of the spectrum, both of which are consequences of temporal averaging. Examination of Fig. 3(c), where the difference between the Fourier transforms of the current obtained using the MFIE and CFIE are plotted, reveals the presence of the principal resonant modes more clearly.

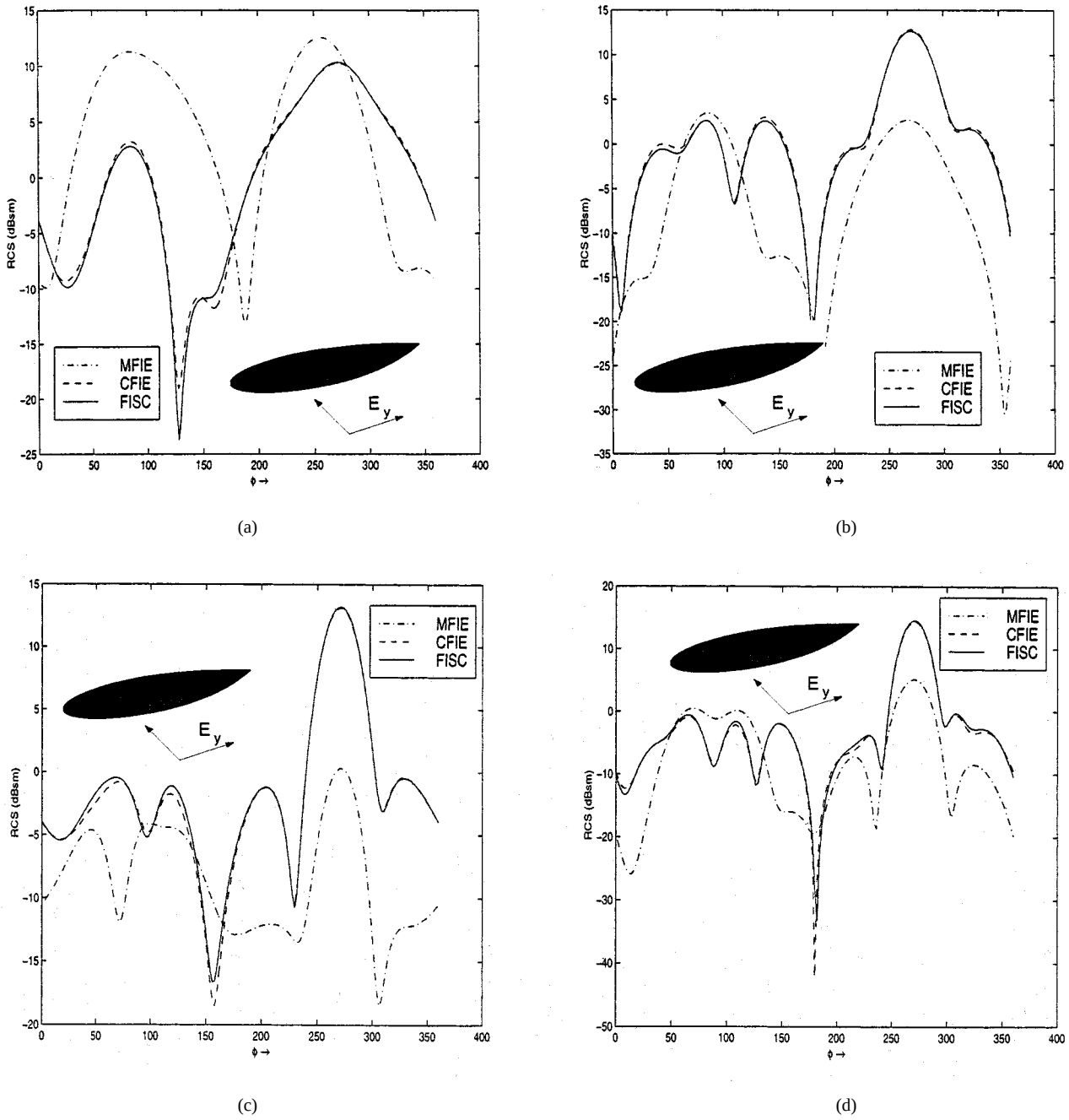

Fig. 7. The radar scattering cross-section of an almond in the x–y plane, extracted from the time-domain CFIE and MFIE is compared to that obtained from FISC for a set of frequencies. The incident wave is $\hat{\boldsymbol{p}} = \hat{\boldsymbol{y}}$ polarized and is traveling in the $\hat{\boldsymbol{k}} = -\hat{\boldsymbol{x}}$ direction. (a) 120 MHz. (b) 150 MHz. (c) 200 MHz. (d) 250 MHz.

In what follows, the RCS patterns obtained using the MFIE and CFIE codes are compared against those obtained using FISC. The RCS patterns obtained using the EFIE codes are not shown as it is well known that, while the currents on the surface computed using the EFIE are corrupted by interior modes, the scattered far-fields obtained from them are not [19]. Fig. 4(a)–(d) compare the RCS pattern in the x–z plane computed using the time-domain CFIE and MFIE codes, FISC, and Mie series solutions at four different frequencies chosen either toward the end of the spectrum or close to a resonance. As is seen in these figures, the time-domain CFIE faithfully reproduces analytical results as well as those obtained from FISC while the MFIE does not. It should be noted that the CFIE results agree reasonably well with those from FISC and Mie methods at both 120 and 280 MHz in spite of the fact that at these frequencies the power in the incident field is down by 45 dB from its peak value. In more quantitative terms, the deviation from Mie solutions at these four frequencies are 28%, 11%, 48%, and 51% for the MFIE results, and 1.7%, 4%, 5%, and 11% for the CFIE results. These results are not surprising, as the existence of nonphysical resonant currents in the solution to the MFIE will cause errors to propagate in any MOT scheme. Thus, when the RCS pattern is extracted from the far-field signature, these errors are most conspicuous at the ends of the band. While comparison of MFIE, CFIE, FISC, and Mie results at other points in the range 140 MHz $\leq f \leq$ 270

MHz are omitted for the sake of brevity, they agree very well with each other as long as f is not close to any of the resonance frequencies.

Next, scattering from a cone-sphere is studied. The cone is 1 m long, the radius of the half-sphere attached to the cone is 0.235 m, and the cone-sphere is discretized with 1656 unknowns. The incident field is a modulated Gaussian pulse with center frequency $f_0 = 400$ MHz and bandwidth $f_{bw} = 350$ MHz; it is $\hat{\boldsymbol{p}} = \hat{\boldsymbol{z}}$ polarized, and is traveling in the $\hat{\boldsymbol{k}} = -\hat{\boldsymbol{x}}$ direction. The RCS patterns in the x–z plane obtained from the time-domain MFIE and CFIE codes are compared against those obtained from FISC for four different frequencies, as shown in Fig. 5(a)–(d). As before, while the results obtained from the CFIE code ($\beta = 1.0$) agree very well with those from FISC for all four frequencies, those obtained from the MFIE code do not. The results obtained using the MFIE code differ from FISC by 48%, 69%, 40%, and 93% while those obtained using the CFIE code differ by 5%, 6%, 6%, and 16%, respectively.

In the next two examples, the scatterer being analyzed is an almond with a maximum height of 0.0575 m, maximum width of 1.15 m, and length of 3 m and is discretized using 1104 spatial unknowns. In the first of these two examples, the incident wave propagates along $\hat{\boldsymbol{k}} = -\hat{\boldsymbol{z}}$, is $\hat{\boldsymbol{p}} = \hat{\boldsymbol{y}}$ polarized, has a center frequency of $f_0 = 200$ MHz, and the bandwidth of $f_{bw} = 150$ MHz. The RCS in the y–z plane is computed and representative results are shown in Fig. 6(a)–(d). The agreement between the results obtained from the time-domain CFIE code ($\beta = 1.0$) and FISC is excellent for a broad range of frequencies, whereas those obtained using the time-domain MFIE differ by as much as 10 dB from those obtained with FISC. Indeed, for the results shown in Fig. 6(a)–(d), the results obtained using the time-domain MFIE code differ from FISC over the range of angles by 64%, 105%, 84% and 67%, whereas those obtained using the time-domain CFIE code differ by 3%, 8%, 3%, and 5%, respectively. Again, only "problematic" frequencies are shown in this and the next example. Similar observations can be deduced from Fig. 7(a)–(d), which compare the RCS patterns in the x–y plane due to a $\hat{\boldsymbol{k}} = -\hat{\boldsymbol{x}}$ propagating and $\hat{\boldsymbol{p}} = \hat{\boldsymbol{y}}$ polarized Gaussian pulse with a center frequency of $f_0 = 200$ MHz and bandwidth $f_{bw} = 150$ MHz. The results obtained using the time-domain MFIE differ from those obtained using FISC by 134%, 135%, 137%, and 93%, while those obtained using the time-domain CFIE code differ by 8%, 5%, 7%, and 15%. It should be pointed out here that it is possible to extract meaningful results from the CFIE time-domain data at 120 MHz in spite of the fact that at this frequency the power of the incident pulse is down by about 46 dB with respect to its peak value.

IV. Conclusions

In this article, a stable MOT scheme for solving a time-domain CFIE has been outlined. It was argued theoretically and demonstrated experimentally that this CFIE permits the computation of resonance-free solutions to scattering problems involving closed objects. Furthermore, it has been shown that the solution to the CFIE is accurate even at frequencies where the the power in the incident pulse is very low. Hence, this CFIE enables the accurate analysis of transient scattering from large and closed bodies, whereas the excitation of the cavity modes often corrupts the solutions to the commonly used EFIE and MFIE. The CFIE-based MOT scheme has been used in conjunction with the recently developed fast time-domain scheme called the PWTD algorithm, making transient analysis of scattering from electrically large objects possible.

Acknowledgment

The authors would like to thank J. M. Song and W. C. Chew for granting access to FISC technology, S. P. Walker for numerous discussions, and the NCSA for access to its computational facilities.

References

[1] E. K. Miller, "A selective survey of computational electromagnetics," *IEEE Trans. Antennas Propagat.*, vol. 36, pp. 1281–1305, Sept. 1988.

[2] D. A. Vechinski and S. M. Rao, "A stable procedure to calculate the transient scattering by conducting surfaces of arbitrary shape," *IEEE Trans. Antennas Propagat.* , vol. 40, pp. 661–665, June 1992.

[3] B. P. Rynne and P. D. Smith, "Stability of time marching algorithms for the electric field integral equations," *J. Electromagn. Waves Applicat.*, vol. 12, pp. 1181–1205, 1990.

[4] A. Sadigh and E. Arvas, "Treating instabilities in matching-on-in-time methods from a different perspective," *IEEE Trans. Antennas Propagat.*, vol. 41, pp. 1695–1702, Dec. 1993.

[5] P. J. Davies, "A stability analysis of a time marching scheme for the general surface electric field integral equation," *Appl. Numer. Math.*, vol. 27, pp. 35–57, 1998.

[6] M. J. Bluck and S. P. Walker, "Time-domain bie analysis of large three dimensional electromagnetic scattering problems," *IEEE Trans. Antennas Propagat.*, vol. 45, pp. 894–901, May 1997.

[7] S. Dodson, S. P. Walker, and M. J. Bluck, "Implicitness and stability of time domain integral equation scattering analysis," *Appl. Comp. Electromagn. Soc. J.*, vol. 13, no. 3, pp. 291–301, 1998.

[8] G. Manara, A. Monorchio, and R. Reggiannini, "A space-time discretization criterion for a stable time-marching solution of the electric field integral equation," *IEEE Trans. Antennas Propagat.*, vol. 45, pp. 527–532, Mar. 1997.

[9] W. Pinello, A. Ruehli, and A. Cangellaris, "Stabilization of time domain solutions of the efie based on the partial element equivalent circuit models," *Proc. IEEE Antennas Propagat. Soc. Int. Symp.*, vol. 3, pp. 966–969, July 1997.

[10] S. M. Rao and T. K. Sarkar, "An efficient method to evaluate the time-domain scattering from arbitrarily shaped conducting bodies," *Microwave Opt. Technol. Lett.*, vol. 17, pp. 321–325, 1998.

[11] K. Aygün, A. A. Ergin, B. Shanker, S. E. Fisher, and E. Michielssen, "Transient analsis of thin wire antennas mounted on three-dimensional perfectly conducting bodies," *14th Annu. Rev. Progress Appl. Computat. Electromagn.*, vol. 2, pp. 838–844, 1998.

[12] B. Shanker, A. A. Ergin, K. Aygün, and E. Michielssen, "Analysis of transient electromagnetics scattering phenomena using a two-level plane wave time-domain algorithm," *IEEE Trans. Antennas Propagat.*, vol. 48, pp. 510–523, Apr. 2000.

[13] ——, "A two-level plane wave time domain algorithm for the fast analysis of transient electromagnetic scattering phenomena," Univ. Illinois Urbana-Champaign, Tech. Rep., 1998.

[14] ——, "Computational complexity and implementation of two-level plane wave time domain algorithm for scalar wave equation," in *Proc. IEEE Antennas Propagat. Int. Symp.*, vol. 2, Atlanta, GA, July 1998, pp. 944–947.

[15] A. A. Ergin, B. Shanker, and E. Michielssen, "Fast evaluation of transient wave fields using diagonal translation operators," *J. Comp. Phys.*, vol. 146, pp. 157–180, 1998.

[16] ——, "The plane wave time domain algorithm for the fast analysis of transient wave phenomena," *IEEE Antennas Propagat. Mag.*, vol. 41, pp. 39–52, Aug. 1999.

[17] P. D. Smith, "Instabilities in time marching methods for scattering: Cause and rectification," *Electromagn.*, vol. 10, pp. 439–451, 1990.

[18] D. S. Jones, *Methods in Electromagnetic Wave Propagation.* Oxford, U.K.: Oxford Sci., 1994.

[19] J. R. Mautz and R. F. Harrington, "H-field, e-field, and combined field solutions for conducting bodies of revolution," *AEÜ*, vol. 32, pp. 157–164, 1978.
[20] A. F. Peterson, "The "interior resonance" problem associated with surface integral equations of electromagnetics: Numerical consequences and a survey of remedies," *J. Electromagn. Waves Applicat.*, vol. 10, pp. 293–312, 1990.
[21] D. A. Vechinski and S. M. Rao, "Transient scattering from dielectric cylinders: E-field, h-field, and combined field solutions," *Radio Sci.*, vol. 27, pp. 611–622, 1992.
[22] S. M. Rao, D. R. Wilton, and A. W. Glisson, "Electromagnetic scattering by surfaces of arbitrary shape," *IEEE Trans. Antennas Propagat.*, vol. 30, pp. 408–418, May 1982.
[23] S. M. Rao and D. R. Wilton, "Transient scattering by conducting surfaces of arbitrary shape," *IEEE Trans. Antennas Propagat.*, vol. 39, pp. 56–61, Jan. 1991.
[24] M. Abramowitz and I. A. Stegun, *Handbook of Mathematical Functions*. New York: Dover, 1972.
[25] Y. Saad, *Iterative Methods for Sparse Linear Systems*. New York: PWS, 1996.
[26] J. M. Song, C. C. Lu, and W. C. Chew, "MLFMA for electromagnetic scattering by large complex objects," *IEEE Trans. Antennas Propagat.*, vol. 45, pp. 1488–1493, Oct. 1997.

Balasubramaniam Shanker (M'96) received the B.Tech. degree from the Indian Institute of Technology, Madras, India, in 1989, and the M.S. and Ph.D. degrees from the Pennsylvania State University, State College, PA, in 1992 and 1993, respectively.

From 1993 to 1996, he was a Research Associate in the Department of Biochemistry and Biophysics, Iowa State University, Ames, where he worked on the molecular theory of optical activity. From 1996 to 1999 he was with the Center for Computational Electromagnetics at the University of Illinois at Urbana-Champaign, first as a Research Associate and then as a Visiting Assistant Professor. He is currently an Assistant Professor in the Department of Electrical and Computer Engineering, Iowa State University. He has published over 35 journal articles and over 40 conference papers/presentations. His research interests include all aspects of computational electromagnetics, with an emphasis on fast time and frequency-domain algorithms.

Dr. Shanker is listed in *Who's Who in Science and Engineering*. He is a member of the IEEE Optical Society of America (OSA) technical societies.

A. Arif Ergin (S'91) received the B.S. degree from the Middle East Technical University, Ankara, Turkey, in 1992, and the M.S. degree from the University of Illinois at Urbana-Champaign, in 1995. He is currently working toward the Ph.D. degree at the University of Illinois at Urbana-Champaign.

He worked as a Design Engineer in ASELSAN Inc., Ankara, Turkey, from 1992 to 1993. He is currently a Research Assistant at the Center for Computational Electromagnetics, University of Illinois. His current research interests include computational methods for analyzing wave propagation and scattering in acoustics and electromagnetics.

Mr. Ergin is a member of ASA.

Kemal Aygün (S'99) received the B.S. degree from the Middle East Technical University, Ankara, Turkey, in 1995, and the M.S. degree from the University of Illinois at Urbana-Champaign, in 1997, both in electrical engineering. He is currently working toward the Ph.D. degree from University of Illinois at Urbana-Champaign.

Since 1995, he has been a Research Assistant at the Center for Computational Electromagnetics, University of Illinois. His research is currently focused on the numerical solution of electromagnetic scattering and radiation problems.

Mr. Aygün is the recipient of the 1999 Computational Science and Engineering Fellowship.

Eric Michielssen (M'95–SM'99) received the M.S. degree in electrical engineering (*summa cum laude*) from the Katholieke Universiteit Leuven (KUL, Belgium), in 1987, and the Ph.D. degree in electrical engineering from the University of Illinois at Urbana-Champaign (UIUC), in 1992.

He served as a Research and Teaching Assistant in the Microwaves and Lasers Laboratory at KUL and the Electromagnetic Communication Laboratory, UIUC, from 1987 to 1988 and from 1988 to 1992, respectively. He joined the Faculty of the Department of Electrical and Computer Engineering in 1993 and was promoted to Associate Professor in 1998. Since 1995 he has served as Associate Director of the Center for Computational Electromagnetics at UIUC. From 1997 to 1999, he served as an associate editor for *Radio Science*. He authored or coauthored over 65 papers and book chapters and over 100 papers in conference proceedings. His research interests include all aspects of theoretical and applied computational electromagnetics and his principal research focus has been on the development of fast-frequency and time-domain integral equation-based techniques for analyzing electromagnetic phenomena and the development of robust genetic algorithm driven optimizers for the synthesis of electromagnetic devices.

Dr. Michielssen received a Belgian American Educational Foundation Fellowship in 1988 and a Schlumberger Fellowship in 1990. He was the recipient of a 1994 Union of Radio Scientists International (URSI) Young Scientist Fellowship, a 1995 National Science Foundation CAREER Award, and the 1998 Applied Computational Electromagnetics Society (ACES) Valued Service Award. Recently, he was named 1999 URSI—United States National Committee Henry G. Booker Fellow and selected as the recipient of the 1999 URSI Koga Gold Medal. He served as the Technical Chairman of the 1997 ACES Symposium and currently serves on the ACES Board of Directors. He is currently an associate editor for the IEEE TRANSACTIONS ON ANTENNAS AND PROPAGATION. He is a member of URSI Commission B.